Nanotechnology **19** (2008) 235402 (5pp) doi:10.1088/0957-4484/19/23/235402

Quantum model of space–charge-limited field emission in a nanogap

W S Koh[1] **and L K Ang**[1,2]

[1] Institute of High Performance Computing, 117528, Singapore
[2] School of Electrical and Electronic Engineering, Nanyang Technological University, 639798, Singapore

E-mail: kohws@ihpc.a-star.edu.sg and elkang@ntu.edu.sg

Received 22 February 2008, in final form 17 April 2008
Published 6 May 2008
Online at stacks.iop.org/Nano/19/235402

Abstract

This paper presents a modified Thomas–Fermi-approximated quantum model for space–charge-limited field emission in a nanogap with metal electrodes, where the image-charge potential (including anode screening), direct tunnelling, space–charge effects and exchange–correlation effects of the tunnelling current are treated in a one-dimensional quantum model. It is found that the traditional Fowler–Nordheim (FN) law (even with the classical model of anode screening) is no longer valid in a nanogap of less than 10 nm. The smooth transition of our proposed model to the traditional FN law extended to large gap spacing is demonstrated. Application of the model to estimate the emission area of an experimental I–V curve in a nanogap is discussed.

(Some figures in this article are in colour only in the electronic version)

1. Introduction

Electron field emission occurs when a high electric field is applied to a surface, which enhances the probability of electron tunnelling through the surface potential barrier by lowering the barrier [1]. In the field of vacuum electronics, the field emission cathode is seen as an alternative to the thermionic cathode, with advantages such as higher local current density (>1 kA cm^{-2}), compactness, higher efficiency and faster turn-on time. Specific applications are as an electron source in flash memory, electron microscopy, MEMS systems, surface conduction electron emitter display by using field emission in a nanogap [2, 3] and high current electron beam for high power microwave sources [4]. For semiconductor devices, field emission is also an important mechanism for thin barriers in metal–semiconductor junctions of highly doped semiconductors, and metal–molecule–metal junctions [5].

For a metallic surface, the field emission current is described by the well-known Fowler–Nordheim (FN) law [6], which (in the form by Murphy and Good [7]) is

$$J_{\mathrm{FN}} = A_{\mathrm{FN}} \frac{E_0^2}{\Phi_{\mathrm{WF}}\, t^2(y)} \exp\left[\frac{-B_{\mathrm{FN}} v(y) \Phi_{\mathrm{WF}}^{3/2}}{E_0}\right], \qquad (1)$$

where $A_{\mathrm{FN}} = 1.5414 \times 10^{-6}$ A eV V^{-2} and $B_{\mathrm{FN}} = 6.8308 \times 10^9$ eV$^{-3/2}$ V m^{-1} are constants, $t^2(y)$ and $v(y)$ are Nordheim parameters (where $y = 3.79 \times 10^{-5}\sqrt{E_0}/\Phi_{\mathrm{WF}}$), Φ_{WF} is the work function and E_0 is the applied electric field. While the traditional FN law (equation (1)) has been widely used for characterizing field emission measurements, its validity depends on the following assumptions: (a) electron emission is near Fermi energy level, (b) the metal is based on the free electron gas model, (c) the surface is flat, (d) the image-charge potential is approximated by $-k/x$ ($k = e^2/16\pi\epsilon_0$), (e) the gap is large (no anode screening) and (f) space–charge effect is ignored. For sharp emitters, it is a common practice to assume that the surface electric field E_0 is enhanced by a factor of β in equation (1).

Compared to a large gap, field emission in a nanogap is seldom studied [8, 9]. Due to the advances in nanotechnology, devices (such as nanogap resistance switches [10, 11] and nanogap scanning probe microscopes [12]) utilizing field emission or tunnelling in nanogaps have been made possible. Characterization of vacuum nanogaps in these nanogap devices is performed by measuring the field emission characteristics [13–15]. Experimental data of field emission in a nanogap as small as about 1 nm is usually fitted using the Simmons model [8] to estimate the emission area. However, the estimation can be unphysical when the area obtained is smaller than the size of an atom [15]. The limitation lies in the assumption in using the classical model of image-charge

potential (with anode screening), which has singularities at the vacuum interfaces of the cathode and anode. Thus the traditional FN law and the Simmons model may not be accurate to describe field emission in a nanogap.

At high current regime, the space–charge effects of the electrons cannot be ignored and the field emission will converge to space–charge-limited (SCL) current (also known as the classical Child–Langmuir (CL) law) [16, 17]:

$$J_{\mathrm{CL}} = \frac{4\epsilon_0}{9}\sqrt{\frac{2e}{m_{\mathrm{e}}}}\frac{V_{\mathrm{g}}^{3/2}}{D^2}, \tag{2}$$

where D is the gap spacing, V_{g} is the gap voltage, e and m_{e} are the charge and mass of the electron, respectively, and ϵ_0 is the free space permittivity. The transition between the traditional classical FN and CL laws in a large gap had been studied numerically [18, 19], and by particle-in-cell simulation [20]. A large-area carbon nanotube cathode operating at SCL regime has also been fabricated recently [21]. For a nanogap, the quantum CL law with new scalings and properties has been studied in steady-state [22–24] and ultrashort-pulse [25] conditions.

Regardless of high or low current operation, a major concern arises on whether the traditional FN law can directly be used to predict the current–voltage (I–V) characteristics of a nanogap. In this paper, we proposed a modified Thomas–Fermi approximated (TFA) quantum model to calculate the I–V characteristics in a nanogap, where the image-charge potential, space–charge field and exchange–correlation effects of the emitted tunnelling current are determined quantum mechanically. A smooth transition to the traditional FN and CL laws at large D will be demonstrated. Application of the proposed model to characterize the I–V measurement will also be discussed.

2. Theory and formulation

Consider a steady-state electron emission current density J propagating in a 1D planar nanogap of spacing D, where the cathode is grounded and the anode is held at a DC voltage V_{g}. We self-consistently include the effects of anode screening by dividing the nanogap and electrodes into three regions. Regions 1 and 3 are semi-infinite jellium regions representing the cathode and anode, respectively. Region 2 is the vacuum region dictating the amount of electrons that can be emitted through a barrier potential, which (in terms of the gap voltage) is

$$\begin{aligned}\bar{V}(\bar{x}) &= \frac{V(x)}{eV_{\mathrm{g}}} \\ &= \phi_{\mathrm{WF}} - \bar{x} + \phi_{\mathrm{ic}} + \phi_{xc} - \phi,\end{aligned} \tag{3}$$

where $\phi_{\mathrm{WF}} = \Phi_{\mathrm{WF}}/eV_{\mathrm{g}}$ is the normalized work function of the cathode, $\bar{x} = x/D$ (the normalized position in the gap) is the normalized 1D applied electric potential of the accelerating nanogap (i.e. linearly proportional to the x coordinate for a flat surface), $\phi_{\mathrm{ic}} = V_{\mathrm{ic}}/V_{\mathrm{g}}$ (<0) is the normalized image-charge potential, and ϕ_{xc} (<0) and ϕ (<0) are, respectively, the normalized exchange–correlation [26] and space–charge potential of the emitted current density at a given V_{g} and D. Note ϕ_{ic}, ϕ_{xc} and ϕ (all depending on $\bar{x}$) are to be solved simultaneously (see below).

Using equation (3), the field emission current density in terms of the classical CL law (equation (2)) is obtained by solving

$$\mu = \frac{eV_{\mathrm{g}}}{J_{\mathrm{CL}}}\int_{-\infty}^{\infty} N(\bar{E}_x)D(\bar{E}_x)\,\mathrm{d}\bar{E}_x, \tag{4}$$

where $N(\bar{E}_x) = \frac{m_{\mathrm{e}}k_{\mathrm{B}}T}{2\pi^2\hbar^3}\ln[1+\exp(\frac{-eV_{\mathrm{g}}\bar{E}_x}{k_{\mathrm{B}}T})]$ is the number of electrons incident along the emission direction x with normalized kinetic energies per unit area ($\bar{E}_x = E_x/eV_{\mathrm{g}}$) between $\bar{E}_x$ and $\bar{E}_x + \mathrm{d}\bar{E}_x$, k_{B} is the Boltzmann constant, and $T = 300$ K is the temperature. The transmission coefficient $D(\bar{E}_x) = \exp[-\frac{2D}{\hbar}\sqrt{2em_{\mathrm{e}}V_{\mathrm{g}}}\int_{\bar{x}_1}^{\bar{x}_2}\sqrt{|\bar{V}(\bar{x})-\bar{E}_x|}\,\mathrm{d}\bar{E}_x]$, is solved by using the Wentzel–Kramers–Brillouin–Jeffreys (WKBJ) method. To be consistent with the FN law, the emission current from the anode has been ignored.

By solving the screened Poisson equation in its Green's function form under the Thomas–Fermi approximation (TFA) [27], we obtain the normalized ground state and zero-field image-charge potential ϕ_{ic} due to Coulomb repulsion of the charges in the cathode, vacuum and anode, which is

$$\phi_{\mathrm{ic}} = -\frac{e}{V_{\mathrm{g}}}\int_0^{\infty} p\,\mathrm{d}p\left[D_{\mathrm{vac}}(p,x) + \frac{1}{2p}\right]. \tag{5}$$

Here, $D_{\mathrm{vac}}(p,x)$ is the longitudinal self-consistent field describing the screened Coulomb interaction between two charges at position x and x', and p is the wavevector along the x direction. The details of the TFA model can be found in [27] and are not discussed here.

For a given normalized current density μ, we use a mean-field quantum model [23] to solve for ϕ_{xc} and ϕ, to account for the effects of exchange–correlation and space–charge field of the emitting current inside the gap as a function of V_{g} and D. The normalized 1D time-independent Schrödinger and Poisson equations are

$$q'' + \lambda^2\left[\phi + \bar{x} - \phi_{xc} - \frac{4}{9}\frac{\mu^2}{q^4}\right]q = 0, \tag{6a}$$

$$\phi'' = \frac{2}{3}q^2, \tag{6b}$$

where q is the normalized wave amplitude, q'' (and ϕ'') denote the second derivative of q (and ϕ) with respect to $\bar{x}$, $\lambda = D/\lambda_o$ is the normalized gap spacing, $\lambda_o = \hbar/\sqrt{2em_{\mathrm{e}}V_{\mathrm{g}}}$ is the electron de Broglie wavelength at V_{g} and $\mu = J/J_{\mathrm{CL}}$ is the normalized electron current density obtained from equation (4). The boundary conditions for equations (6*a*) and (6*b*) are $q(1) = \sqrt{2\mu/3}$, $q'(1) = 0$, $\phi(0) = 0$, $\phi(1) = 0$, $\phi'(1) = s_{\mathrm{a}}$ and $\phi'(0) = s_{\mathrm{c}}$, where s_{a} and s_{c} are, respectively, the calculated surface electric field of the anode and cathode at a given μ.

By considering both electrodes are barium (Ba) with $E_{\mathrm{F}} = 2.317$ eV and $\Phi_{\mathrm{WF}} = 2.48$ eV [28], we solve the I–V characteristics of electron emission in a nanogap for the following four systems: (i) the classical Ba–vacuum system, (ii) the classical Ba–vacuum–Ba system including the

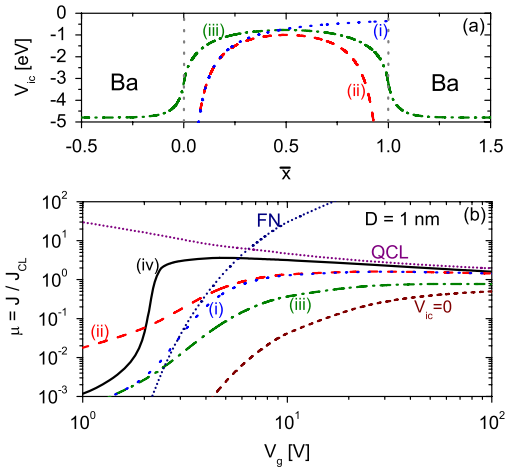

Figure 1. (a) The image-charge potential V_{ic} for the Thomas–Fermi approximated (TFA) quantum Ba–vacuum–Ba system (dashed–dotted line), the classical Ba–vacuum–Ba system (dashed line) and the classical Ba–vacuum (dotted line) system, respectively, for a 1 nm nanogap of barium electrodes ($E_F = 2.317$ eV and $\Phi_{WF} = 2.48$ eV). (b) The normalized electron emission current density $\mu = J/J_{CL}$ as a function of $V_g = 1$–100 V at $D = 1$ nm for (i) the classical Ba–vacuum system (dotted line), (ii) the classical Ba–vacuum–Ba system (dashed line), (iii) the TFA quantum Ba–vacuum–Ba system (dashed–dotted line) and (iv) the modified TFA quantum Ba–vacuum–Ba system (solid line), respectively. The short-dotted lines represent the well-known Fowler–Nordheim (FN) law without space–charge effects [7] and the quantum Child–Langmuir (QCL) law [23]. The short-dashed line denotes the case of a simple triangular barrier with zero image-charge potential $V_{ic} = 0$.

anode screening effect in the classical image-charge potential, (iii) the TFA quantum Ba–vacuum–Ba system ($\phi_{xc} = 0$) and (iv) the modified TFA quantum Ba–vacuum–Ba system. Note that space–charge effects are included self-consistently in all calculations. To obtain the I–V characteristics self-consistently for each system, we first solve equation (4) to obtain the normalized electron current density μ for a given potential profile given by equations (3) and (5). Substituting μ into equations (6), we obtain the corresponding normalized space–charge potential ϕ and exchange–correlation potential ϕ_{xc}, to update equations (3) and (4). A self-consistent solution of μ, which gives the corresponding self-consistent ϕ and ϕ_{xc}, is thus obtained by solving equations (3)–(6) iteratively for given V_g and D.

3. Results and discussion

In figure 1(a), it is shown that the TFA image-charge potential (solid line) is continuous at both metal–vacuum interfaces for $D = 1$ nm by including the influence of anode screening. For classical image-charge potentials either with or without the anode screening (dashed and dotted lines), the singularity of V_{ic} at the metal–vacuum interfaces may cause an underestimation of the barrier width especially when the applied voltage is low. Figure 1(b) shows the I–V curves of a 1 nm gap with Ba cathode and Ba anode are computed for the four systems (solid lines) mentioned above. The dashed–dotted and dotted lines are the FN law (equation (1)) and the quantum CL law [23], respectively. The case of a triangular barrier where there is no image-charge lowering or $V_{ic} = 0$ (dashed line) is also plotted for comparison.

By comparing the classical Ba–vacuum system (i) and the FN law (dotted line), it is observed that the contributions of direct tunnelling increases substantially at small voltage (<2 V) for a 1 nm gap. This finding shows that electrons with energy smaller than the Fermi energy contribute significantly to the field emission in a nanogap if the image-charge lowering is taken into account.

In the classical Ba–vacuum–Ba system (ii), the image-charge lowering effect (due to anode screening as considered by Simmons [8]) at the vacuum–anode interface produces a smaller barrier as compared to the classical Ba–vacuum system. The smaller barrier will result in a significantly higher current density especially in the regimes of direct tunnelling and field emission. Thus, if emission area is evaluated based on such a high calculated current (as compared to the other three cases—(i), (iii) and (iv)), the emission area estimated may become an unphysical value.

The absence of the singularity at both the metal–vacuum interfaces in the TFA quantum model (iii) will produce a wider potential barrier and thus a smaller current density compared to classical models. However, if we focus on the high current regime (i.e. >10 V), we will find that the TFA model curve (iii) does not revert back to $\mu = 1$ (i.e. the classical SCL limit as $D \gg \lambda_o$) as we would expect when the voltages become very large for such a small gap. Therefore, the I–V curves produced by the TFA quantum model is insufficient to give us the correct picture.

Interestingly, the missing link stems from the fact that we did not consider the exchange–correlation potential due to the intense interactions between the electrons in the nanogap through a self-consistent fashion. By including the exchange–correlation potential in the self-consistent manner as detailed in section 2, the modified TFA quantum system (iv) has a larger current density approaching the quantum CL law in the high voltage regime. Note this barrier lowering effect from the exchange–correlation term of the emitted current becomes dominant only at very small D (<10 nm) (see below).

Figure 2 illustrates the calculated normalized electron exchange–correlation, space–charge and barrier potentials from the modified TFA quantum model at $V_g = 1$, 4 and 40 V, which represent the transition from direct tunnelling to field emission and space–charge-limited (SCL) regimes. The normalized exchange–correlation and space–charge potentials of the electron current are dominant in the transition regime between the FN and SCL regimes at $V_g = 4$ V, as shown in figures 2(a) and (b). Therefore, in the FN and SCL regimes, the influence of the exchange–correlation potential is negligible. At $V_g = 1$ V, the space–charge effect is not important ($-\phi = 0$) as expected. The variation of the normalized potential barrier, as shown in figure 2(c), will vastly affect the I–V characteristics in the different voltage regimes.

In figure 3, we show the convergence of the modified TFA quantum system (solid lines) to the classical models bounded

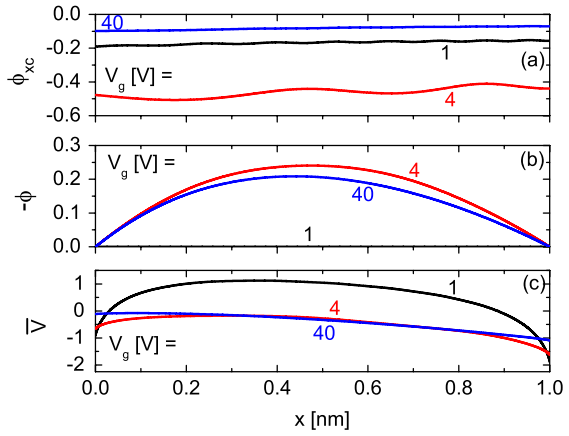

Figure 2. The normalized profile of (a) electron exchange–correlation potential $[-\phi_{xc}]$, (b) space–charge potential $[-\phi]$ and (c) barrier potential $[V]$, in the nanogap with $D = 1$ nm at different operating regimes: direct tunnelling to field emission ($V_g = 1$ V), field emission to space–charge-limited current (4 V) and space–charge-limited current (40 V).

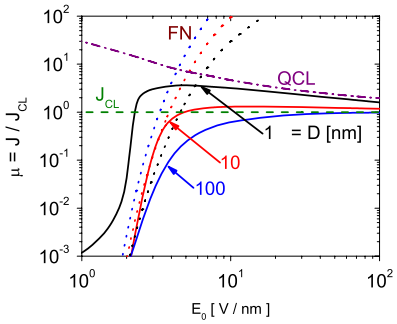

Figure 3. The normalized electron current density $\mu = J/J_{\mathrm{CL}}$ as a function of the applied electric field $E_0 = V_g/D = 1$–100 V nm^{-1} for the modified TFA quantum Ba–vacuum–Ba system at $D = 1$, 10 and 100 nm (top to bottom). The dotted lines are the traditional (normalized) Fowler–Nordheim law ($J_{\mathrm{FN}}/J_{\mathrm{CL}}$) without space–charge effects at $D = 1$, 10 and 100 nm (right to left) The classical and quantum Child–Langmuir law are also plotted as the dashed line and dashed–dotted line, respectively.

by the classical FN law (dotted lines) and the CL law: classical (dashed line) and quantum (dashed–dotted line) when D is increased from 1 to 100 nm. A small deviation of the field emission current at the low voltage regime (<2 V) is attributed to the assumption that the classical image-charge potential (k/x) is used to derive the traditional FN law (dotted lines), whereas our model will converge to the image-charge potential $k/(x + x_o)$ for large D [27, 30]. We would also like to point out that the current contributed by direct tunnelling disappears at $D = 100$ nm.

Figure 4 shows the normalized electron current density $\mu = J/J_{\mathrm{CL}}$ as a function of $V_g = 1$–100 V at $D = 1$ nm for the modified TFA quantum Ba–vacuum–Ba/Ba–vacuum–W and W–vacuum–W/W–vacuum–Ba systems at $D = 1$ nm. The Fermi energy and work function of tungsten (W) used in the calculations are $E_{\mathrm{F}} = 5.782$ eV and $\Phi_{\mathrm{WF}} = 4.4$ eV, respectively [28]. It is observed that the main electron emission characteristic is primarily determined by the cathode material

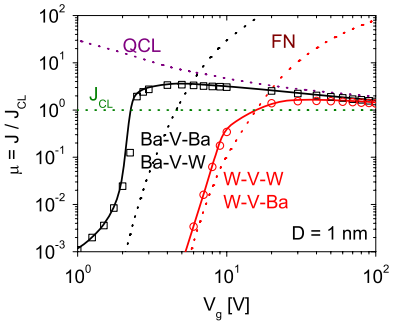

Figure 4. The normalized electron current density $\mu = J/J_{\mathrm{CL}}$ as a function of $V_g = 1$–100 V at $D = 1$ nm for the modified TFA quantum Ba–vacuum–Ba/Ba–vacuum–W (left) and W–vacuum–W/W–vacuum–Ba (right) systems at $D = 1$ nm. The symbols show calculations using the Miller–Good form of the transmission coefficient for comparison. The dotted lines are the traditional (normalized) Fowler–Nordheim law ($J_{\mathrm{FN}}/J_{\mathrm{CL}}$) for Ba–vacuum (left dotted) and W–vacuum (right dotted) systems at $D = 1$ nm. The classical and quantum Child–Langmuir law are also plotted as the dashed line and dashed–dotted line, respectively. The results for Ba–vacuum–Ba coincides with Ba–vacuum–W, and W–vacuum–W coincides with W–vacuum–Ba too. The Fermi energy and work function of tungsten (W) are $E_{\mathrm{F}} = 5.782$ eV and $\Phi_{\mathrm{WF}} = 4.4$ eV, respectively [28].

(as shown from the overlaps of the I–V characteristics of the Ba–vacuum–Ba and Ba–vacuum–W (W–vacuum–W and W–vacuum–Ba) systems). In the figure, it is interesting to note that the I–V curves of the W emitter (calculated using the modified TFA model) approach that of the traditional FN curve in the low voltage regime, whereas the deviation from the traditional FN law is much larger for Ba. The shift of the I–V curve towards the traditional FN law is attributed to the larger work function of W as compared to Ba. The I–V curves for both barium and tungsten systems calculated with the WKBJ (solid lines) and the Miller–Good [29] (symbols) form of the transmission coefficient are also plotted for comparison. Note that there are little discrepancies between the use of the WKBJ or the Miller–Good approximations. The largest discrepancy occurs near the boundary of the field emission and the transition regime where the WKBJ approximation tends to overestimate the contribution from the thermal tail of the function $N(\bar{E}_x)$ in equation (4) as expected.

We have also used our model (modified TFA quantum model) to estimate the electron emission area based on a recent experimental I–V curve (copper cathode) in a gap spacing for $D = 1.0 \pm 0.2$ nm [15]. It was reported that the best fit of the experimental results by using the Simmons model (similar to the classical metal–vacuum–metal system) is at $D = 0.8$ nm with an emission area of 0.004 nm^2, which is smaller than the size of one atom, and thus was believed to be non-physical [8]. Using our models, our estimation area is about 1.2 nm^2 (at $D = 0.8$ nm) and 100 nm^2 (at $D = 1$ nm, which is the mean value of the measured D in [15]). Note the Fermi energy E_{F} and work function ϕ_{WF} is assumed to be 4.76 eV and 7.034 eV, respectively, in this calculation [28]. Thus, our model may be used as a more accurate tool to characterize the gap spacing or emission area for sub-10 nm spacing electrodes in nanofabrication.

4. Conclusion

In summary, we have formulated a 1D modified TFA quantum model to predict the field emission behaviour of a sub-10 nm gap of metallic electrodes, including the effects of anode screening, direct tunnelling, electron exchange–correlation and space–charge effects of the emitting electron current density in the nanogap. Comparisons with the classical and TFA models are shown and the importance of including and determining a self-consistent exchange–correlation potential in the calculations are discussed. The convergence of our modified TFA quantum model to the classical FN law and CL law at large gap spacing is also demonstrated. Finally, we have used our model to estimate the emission area of a nanogap and obtained a much more credible estimation as compared to the estimation by the classical Simmons model.

Acknowledgments

This work is supported by the Joint Research Laboratory on Computational Nanoelectronics and Plasmonics between the Institute of High Performance Computing and Nanyang Technological University. In addition, LKA was supported by the Agency for Science, Technology and Research of Singapore (042 101 0080) and USA AFOSR AOARD grant (06-4050).

References

[1] Gadzuk J W and Plummer E W 1973 *Rev. Mod. Phys.* **45** 487
[2] Oguchi T, Yamaguchi E, Sasaki K, Suzuki K, Uzawa S and Hatanaka K 2005 *SID Symp. Digest* **36** 1929
[3] Lo H-Y, Li Y, Chao H Y, Tsai C-H and Pan F-M 2007 *Nanotechnology* **18** 475708
[4] Jensen K L 1999 *Phys. Plasmas* **6** 2241
[5] Beebe J M, Kim B, Gadzuk J W, Frisbie C D and Kushmerick J G 1999 *Phys. Rev. Lett.* **97** 026801
[6] Fowler R H and Nordheim L 1928 *Proc. R. Soc. London* A **117** 173
[7] Murphy E L and Good R H Jr 1956 *Phys. Rev.* **102** 1424
[8] Simmons J G 1963 *J. Appl. Phys.* **34** 1793
[9] Koh W S and Ang L K 2006 *Appl. Phys. Lett.* **89** 183107
[10] Naitoh Y, Horikawa M, Abe H and Shimizu T 2006 *Nanotechnology* **17** 5669
[11] Blom Y T, Welch K, Strϕmme M, Coronel E and Leifer K 2007 *Nanotechnology* **18** 285301
[12] Nagase M and Yamaguchi H 2007 *J. Phys.: Conf. Ser.* **61** 856
[13] Steinmann P and Weaver J M R 2004 *J. Vac. Sci. Technol.* B **22** 3178
[14] Negishi R, Hasegawa T, Terabe K, Aono M, Ebihara T, Tanaka H and Ogawa T 2006 *Appl. Phys. Lett.* **88** 223111
[15] Gupta R and Willis B G 2007 *Appl. Phys. Lett.* **90** 253102
[16] Child C D 1911 *Phys. Rev. (Series I)* **32** 492
[17] Langmuir I 1913 *Phys. Rev.* **2** 450
[18] Lau Y Y, Liu Y F and Parker R K 1994 *Phys. Plasmas* **1** 2082
[19] Jensen K L, Kodis M A, Murphy R A and Zaidman E G 1997 *J. Appl. Phys.* **82** 845
[20] Feng Y and Verboncoeur J P 2006 *Phys. Plasmas* **13** 073105
[21] Shiffler D, Zhou O, Boer C, Lacour M and Golby K 2005 *IEEE Trans. Plasma Sci.* **32** 2152
[22] Lau Y Y, Chernin D, Colombant D G and Ho P-T 1991 *Phys. Rev. Lett.* **66** 1446
[23] Ang L K, Kwan T J T and Lau Y Y 2003 *Phys. Rev. Lett.* **91** 208303
[24] Ang L K, Koh W S, Lau Y Y and Kwan T J T 2006 *Phys. Plasmas* **13** 056701
[25] Ang L K and Zhang P 2007 *Phys. Rev. Lett.* **98** 164802
[26] Pedrew J P and Wang Y 1992 *Phys. Rev.* B **45** 13244
[27] Il'chenko L G and Goraychuk T V 2001 *Surf. Sci.* **478** 169
[28] Jensen K L 2000 *J. Appl. Phys.* **88** 4455
[29] Miller S C and Good R H 1953 *Phys. Rev.* **91** 174
[30] Lang N D and Kohn W 1973 *Phys. Rev.* B **7** 3541